Journal of Non-Crystalline Solids 473 (2017) 96–101

Contents lists available at ScienceDirect

Journal of Non-Crystalline Solids

journal homepage: www.elsevier.com/locate/jnoncrysol

Improvement of dynamic notch toughness for the $Zr_{56}Co_{28}Al_{16}$ bulk metallic glass by local pre-deformation

J. Gu[a], T.W. Zhang[b,c], Z.M. Jiao[b,c], Z.Y. Wang[a,*], Z.H. Wang[b,c,**], W. Ma[d], J.W. Qiao[e]

[a] College of Mechanics, Taiyuan University of Technology, Taiyuan 030024, China
[b] Institute of Applied Mechanics and Biomedical Engineering, Taiyuan University of Technology, Taiyuan 030024, China
[c] Shanxi Key Laboratory of Material Strength and Structural Impact, Taiyuan University of Technology, Taiyuan 030024, China
[d] Institute of Mechanics, University of the Chinese Academy of Sciences, Beijing 100190, China
[e] College of Materials Science and Engineering, Taiyuan University of Technology, Taiyuan 030024, China

ARTICLE INFO

Keywords:
Bulk metallic glass
Local pre-deformation
Pre-existing shear bands
Dynamic notch toughness

ABSTRACT

Mode I dynamic three-point bending fracture tests are conducted on both as-cast and local pre-deformed $Zr_{56}Co_{28}Al_{16}$ bulk metallic glass specimens. Similar to quasi-static cases, the notch toughness of the pre-compressed specimens is improved compared with that of as-cast ones upon dynamic loadings, which is mainly attributed to the fact that the pre-compression can produce numerous shear bands, especially for main shear band, guiding and deflecting the cracks. In addition, the crack patterns and fractography are analyzed to evaluate the influence of local pre-existing shear bands on the dynamic fracture toughness.

1. Introduction

Bulk metallic glasses (BMGs) have been of significant interest owing to their amorphous structure as well as a wide range of desirable mechanical properties, such as superior strength, high hardness, great elastic limit, excellent wear and corrosion resistance [1–5]. However, the limited ductility of BMGs is taken as an obstacle to prevent their widespread usage [6,7]. Therefore, designing BMG components on the basis of strength is not appropriate since it may lead to low reliability [8]. A more appropriate way is to use the “defect tolerant” fracture mechanics approach, and fracture toughness has become an important parameter [9]. However, the plastic flow in BMGs at ambient temperature is highly localized in shear bands, the macroscopic deformation is not well distributed among many shear bands, then cracks will initiate and rapidly propagate, which leads to catastrophic fracture [10]. If the formation of multiple shear bands is stimulated under the external force, the stress concentration can be mitigated, resulting in higher toughness [11]. Actually, composition optimization has been used to develop tough monolithic BMGs and BMG matrix composites. Because ductile dendrites in BMG matrix composites can stabilize BMGs against the catastrophic fracture, producing graceful failure [11–14]. The finite-element simulation results based on the Mohr–Coulomb-based constitutive model demonstrate that the extent of the plastic zone and the multiplication of shear bands ahead of a notch tip will be enhanced by a higher Poisson ratio [15]. However, the insensitivity of the Poisson ratio to the fracture toughness has been reported in some Ni-based BMGs [16,17].

Previous studies have shown that pre-deformation induced pre-existing shear bands can change the mechanical properties of BMGs. For example, prior plastic deformation process was utilized to tune the mechanical performance of $Ti_{40}Zr_{25}Ni_3Cu_{12}Be_{20}$ BMG [18]. Furthermore, pre-deformation changes the mechanical heterogeneity, i.e., distribution of soft and hard regions in the $Zr_{65}Cu_{15}Al_{10}Ni_{10}$ BMG [19]. In addition, the plasticity of $Zr_{46.75}Ti_{8.25}Cu_{7.5}Ni_{10}Be_{27.5}$ [20], $Zr_{56}Co_{28}Al_{16}$, and $Zr_{65}Ni_{10}Cu_{15}Al_{10}$ [21] BMGs was enhanced by pre-deformation treatments. The molecular-dynamic simulations reveal that plasticity and strength can be effectively improved by pre-introduced shear bands [22]. However, the compressive and tensile mechanical properties of BMGs [23,24] were influenced by the pre-introduced shear bands direction. Besides, the plasticity of BMGs was improved by the pre-introduced shear bands with the orientation parallel to the direction of maximum shear stress [25].

Pre-deformation process was also utilized to improve the fracture toughness of BMGs [10,26,27]. In order to promote numerous shear bands along the main crack, crack bifurcation, and a tortuous crack path, cold rolling is used to improve the mode I fracture toughness of the Zr-based BMG [10]. Indeed, pre-deformation by the compression can improve the notch toughness of both brittle and tough BMGs under

* Corresponding author.
** Corresponding author at: Institute of Applied Mechanics and Biomedical Engineering, Taiyuan University of Technology, Taiyuan 030024, China.
E-mail addresses: wangzhiyong@tyut.edu.cn (Z.Y. Wang), wangzh@tyut.edu.cn (Z.H. Wang).

http://dx.doi.org/10.1016/j.jnoncrysol.2017.07.034
Received 25 April 2017; Received in revised form 29 June 2017; Accepted 30 July 2017
Available online 02 August 2017

quasi-static conditions, Yi et al. [26] fabricated pre-existing shear bands ahead of the notch to provide internal weak interface in a bulk material that guide and deflect the evolving cracks, thereby increasing the crack resistance. Furthermore, the controlled stress wave loading experiments induced sub-critical levels of damage in a notched tough Zr-based BMG show several attempts of the blunting at the moment of crack initiation. The initial sub-critical damage around the notch can increase the energy required for catastrophic failure, which is similar to the improvement in the effective notch radius [27–29]. However, whether the local pre-deformation will alleviate the local stress concentrations and produce an increase in toughness for brittle BMGs under dynamic conditions has not been studied. In this study, the dynamic three-point bending fracture experiments are conducted to investigate the effect of local pre-deformation on the dynamic notch toughness of the brittle $Zr_{56}Co_{28}Al_{16}$ metallic glass.

2. Experimental procedures

2.1. Specimen preparation

The $Zr_{56}Co_{28}Al_{16}$ (ZC) specimens are prepared by arc melting the mixtures of Zr, Co, and Al with high-purity (> 99.9%) in a Ti-gettered argon atmosphere, and subsequent suction casting into a copper mold at a cooling rate of 10^2 k/s. The as-cast specimens with dimensions of 23 mm × 4 mm × 2 mm are cut from the as-cast plates using wire-cut electrical discharge machining (WEDM) and polished to a mirror finish. The full amorphous nature of the as-cast ZC is confirmed by the scanning electron microscope (SEM) and the X-ray diffraction (XRD). Fig. 1 shows the SEM image and XRD pattern of the present alloy. The samples are then pre-notched to a depth of about 2 mm using WEDM, see specimen (A) in Fig. 2(a). Pre-compression shown in Fig. 2(a) is conducted using a CMT5105A servo-hydraulic testing machine under displacement control at a rate of 0.09 mm/min at room temperature before dynamic three-point bending experiments. During compression tests, the threshold deformation is determined by the applied loading. The applied loadings are adopted to be 1.5 kN and 2.5 kN, respectively, Once the applied loading is reached, the sample will be unloaded immediately. In addition, pre-existing shear bands are only introduced near the notch root, in which the stress concentration is available, see specimen (B) in Fig. 2(a). The opposing edges of the notch have always been parallel to each other during pre-compression tests, and the compressed faces of the samples are also parallel to the compression anvils. The crack patterns and fractography are observed by SEM. To confirm the reproducibility of the experimental results, at least three samples are tested for each loading case.

2.2. Dynamic experimental tests

The impact loading experiment device, based on the modified split Hopkinson pressure bar, consists of a projectile, an incident bar, a fixture, a laser velocity measuring device and a data acquisition system (Fig. 2(b)). The projectile and the incident bar are cylindrical, 5 mm in diameter and 80 mm and 500 mm in length, respectively. The incident bar is instrumented by strain gauges 1 at the mid-span of the incident bar. The output signals measured by the strain gauges 1 are recorded at a sampling rate of 0.1 μs. By the strain gauges 1, the incident strain $\varepsilon_i(t)$ and the reflected strain $\varepsilon_r(t)$ in the incident bar are measured. Then, according to the one-dimensional elastic stress wave theory, the input load of the specimen $P(t)$ and the displacement of the bar edge initially in contact with the specimen, $u(t)$, can be calculated according to the following formulas [30]:

$$p(t) = EA(\varepsilon_i(t) + \varepsilon_r(t)) \tag{1}$$

$$u(t) = c_0 \int_0^t (\varepsilon_i(\tau) + \varepsilon_r(\tau))d\tau \tag{2}$$

where A and E are the cross sectional area and elastic modulus of the incident bar respectively. c_0 is the one-dimensional elastic wave velocity. The parameter values of the dynamic experimental tests are summarized in Table 1.

2.3. Determination of fracture toughness

The evaluation of the dynamic fracture initiation toughness of the material involves two key factors: the calculation of the dynamic stress intensity factor (DSIF) and the determination of the fracture initiation time. The spring-mass model is used in calculating the DSIF, $K_I^d(t)$ [30]:

$$K_I^d(t) = \frac{3S\sqrt{a}}{2BW^2} Y\left(\frac{a}{W}\right)\omega_1 \int_0^t p(\tau)\sin\omega_1(t-\tau)d\tau \tag{3}$$

where S, a, B and W are the specimen span, notch depth, thickness and

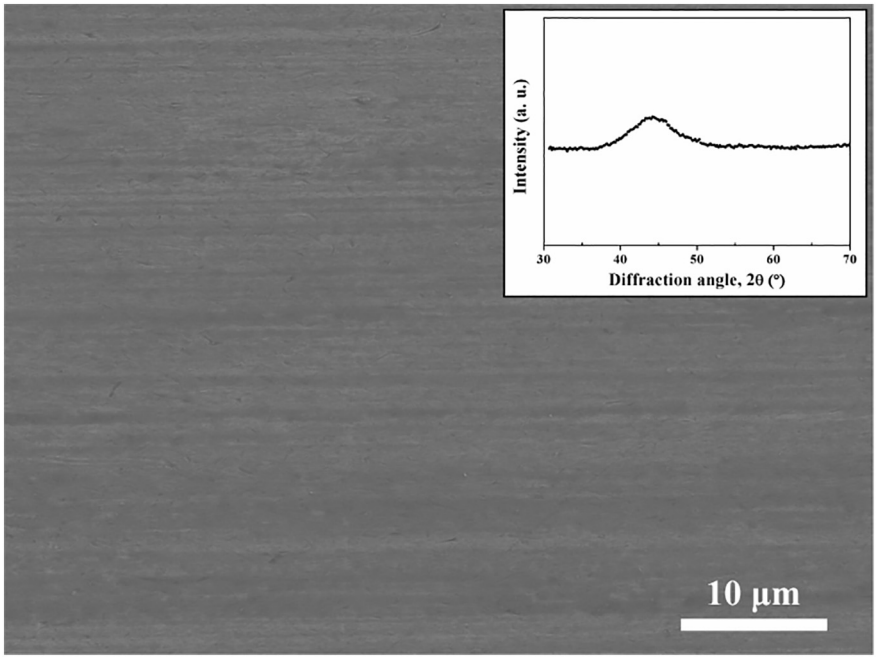

Fig. 1. SEM image and XRD pattern of $Zr_{56}Co_{28}AL_{16}$ BMG.

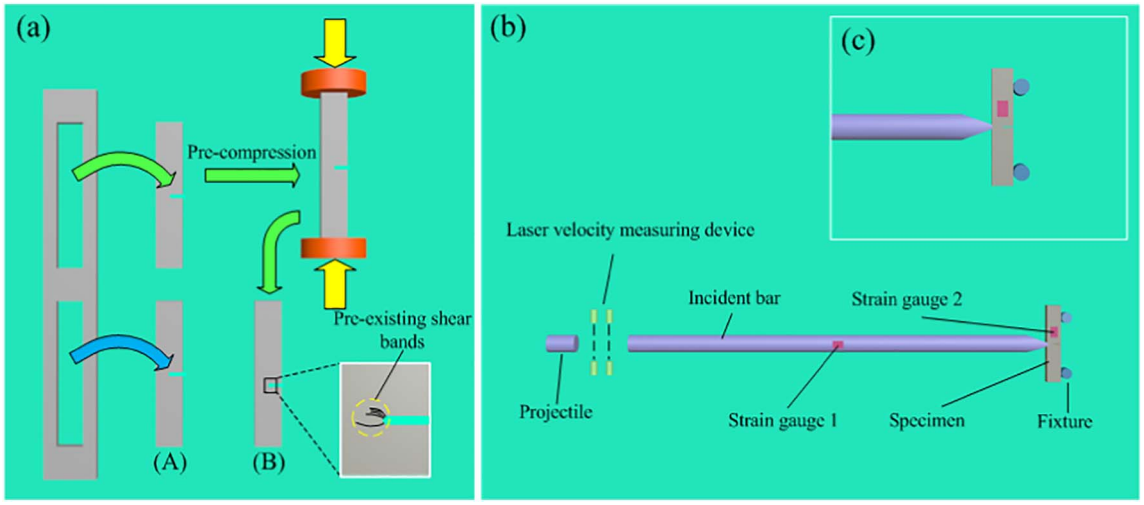

Fig. 2. Schematic diagrams of preparation of $Zr_{56}Co_{28}Al_{16}$ BMG and experimental configuration. (a) The solid yellow arrows indicate the pre-compression loading direction. The enlarged view of the notch root region shows the pre-existing shear bands introduced by pre-compression with a load of 2.5 kN. (b) Modified split Hopkinson pressure bar device. (c) Details of the specimen clamped on the fixture. (For interpretation of the references to colour in this figure legend, the reader is referred to the web version of this article.)

Table 1
The parameter values of the dynamic experimental tests.

Parameter	A (m^2)	E (GPa)	P (kg/m^3)	c_0 (m/s)
Value	1.96×10^{-5}	200	7800	5063

width, respectively. $\omega_1 = \sqrt{K(\alpha)/m_e}$ is the natural frequency of the system. Details are described in the literature [30].

3. Results and discussions

To determine the time of crack initiation (t_f), the strain gauge 2 is used (Fig. 3(a)). The strain gauge 2 is bonded near the notch root at a distance of about 2 mm [30–33] (Fig. 2(b)). The unloading wave propagating from the center position of crack tip of the specimen to strain gauge 2 takes about Δt ($\Delta t = \sqrt{r^2 + (B/2)^2}/c_0 \approx 0.456$ μs, r is the distance between strain gauge 2 and notch root). Thus, the crack initiation time is $t_f = t_{rise} - \Delta t$ (t_{rise} corresponds to the time when voltage begins

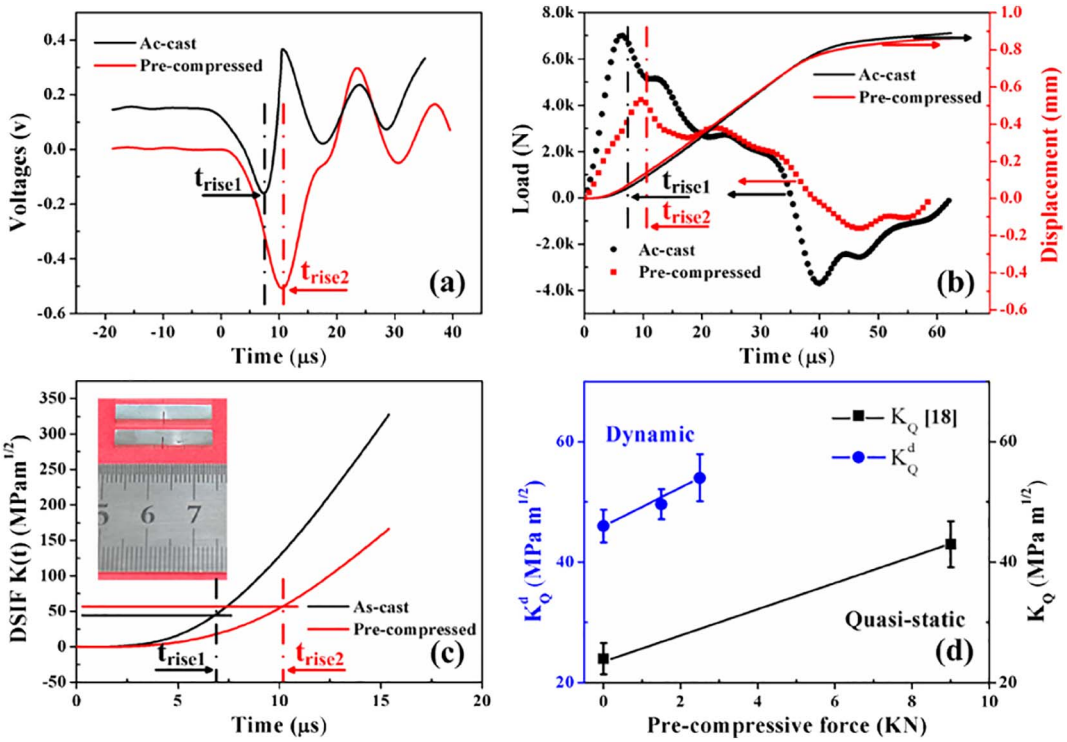

Fig. 3. Experimental results for as-cast and pre-compressed specimens. (a) Strain gauge signals are used to determinate the time to fracture. (b) Load and displacement versus time curve for dynamic single notched three point bending experiments. (c) Experimental determination of the stress intensity factors. (d) Comparison between quasi–static and dynamic notch toughness of as-cast and pre-compressed specimens with different pre-compressive loads.

Table 2
Experimental results for $Zr_{56}Co_{28}Al_{16}Zr_{56}Co_{28}Al_{16}$ bulk metallic glass.

Specimen	Size (mm)	a_0 (mm)	v (m/s)	p_{maxx} (KN)	t_f (μs)	$K_Q{}^d$ (MPa·m$^{1/2}$)	$\dot{K}_Q^d$ (MPa·m$^{1/2}$/s)	2.5 $(K_Q{}^d/\sigma_y)$ (mm)
As-cast	1.99 × 4.13 × 22.19	2.02	30.26	7.01	6.87	46.06	6.71×10^6	1.38
Pre-compressed	1.95 × 4.13 × 22.19	2.05	30.78	4.23	10.07	54.44	5.40×10^6	1.93

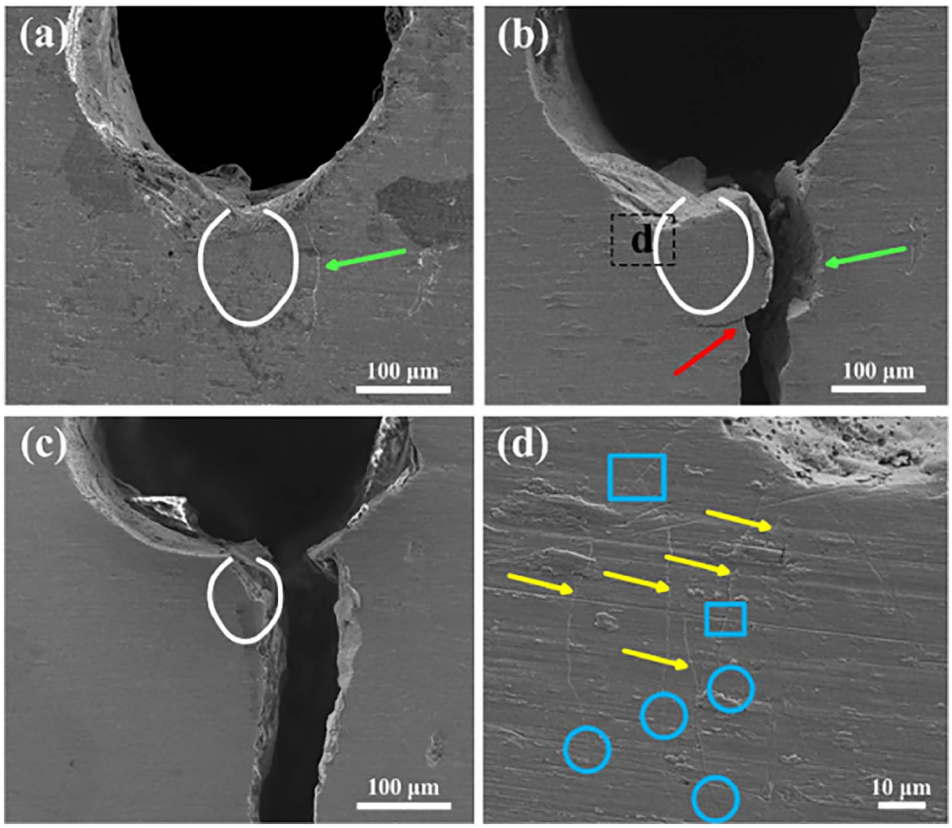

Fig. 4. SEM images of the side views of as-cast and pre-compressed specimen. (a) Pre-existing shear bands introduced by pre-compression. (b) Crack along a main shear band, the bifurcation of the crack, as shown by the red arrow. (c) Cracks of the as-cast specimen are not deflected beyond the as-cast plastic zone size. (d) Secondary shear bands are marked by yellow arrows. (For interpretation of the references to colour in this figure legend, the reader is referred to the web version of this article.)

to rise).

The experimental results are summarized in Table 2, the parameters v, p_{max}, $K_Q{}^d$, and $\dot{K}_Q^d$ denote, respectively, the impact velocity, maximum load, dynamic notch toughness, and stress-intensity-factor rate, which is determined by [30].

The calculated dynamic notch toughness conforms to the validity of $K_Q{}^d$ (i.e. B and $a \geq 2.5\ (K_Q{}^d/\sigma_y)$) [28,34]. Fig. 3(a) shows the crack initiation times of as-cast specimen and pre-compressed one, i.e. t_{rise1} and t_{rise2}, respectively. It is interesting to note that the crack initiation time of the pre-compressed specimen is postponed compared to that of the as-cast one, which is mainly attributed to the blunting induced by pre-existing shear bands at the moment of crack initiation [27]. Fig. 3(b) exhibits the variations of load and displacement with the time for dynamic single-edge notched three-point bending experiments. It is noted that the crack initiation load of pre-compressed specimen is decreased, but descending rate of applied load is reduced after cracking. Actually, the crack propagation is effectively arrested by pre-existing shear bands during deformation upon dynamic loadings [27]. Although subjected to the different applied loads, the displacements along the loading direction of the as-cast and pre-compressed specimens are basically overlapped, as shown in Fig. 3(b). Fig. 3(c) presents the experimental determination of the DSIF of the as-cast and pre-compressed specimens. It is noted that the DSIF of as-cast specimen is always larger than those of pre-compressed ones. The dynamic notch toughness of pre-compressed specimens is slightly higher than that of as-cast ones due to the increase of the energy required for catastrophic specimen failure, which is consistent with an increase in the effective notch radius due to pre-existing shear bands [27]. The inset in Fig. 3(c) shows the as-cast and pre-compressed specimens before three-point bending experiments. Fig. 3(d) reveals the comparison between quasi-static [26] and dynamic notch toughness of as-cast and pre-compressed ZC BMGs with different pre-compressive loads. It can be clearly seen that upon quasi-static loadings, the notch toughness of as-cast specimens is increased with the pre-compressive force [26]. In comparison, upon dynamic loadings, the variation of the notch toughness with the pre-compressive force exhibits a similar tendency, and the value of the notch toughness under dynamic loadings is apparently larger than that under quasi-static cases. The present results demonstrate that the pre-compression can effectively enhance the fracture resistance of ZC BMGs, mainly due to the fact that the pre-existing shear bands can guide and deflect cracks under quasi-static and dynamic conditions [26].

Fig. 4 shows the SEM images of side views of the pre-compressed specimen before (Fig. 4(a)) and after (Fig. 4(b)) the impact experiments. As seen in Fig. 4(b), the crack is deflected beyond the plastic zone size ($R_p = (K_Q{}^d/\sigma_y)^2/2\pi = 123$ μm), and propagated along the pre-existing main shear band. However, as shown in Fig. 4(c), the crack of the as-cast specimen is not deflected beyond the plastic zone size ($R_p = (K_Q{}^d/\sigma_y)^2/2\pi = 88$ μm). The improvement in notched toughness is consistent with other works on the toughness of the BMGs [26,35,36]. A comparison of Fig. 4(a) and (b) indicates that the crack propagating

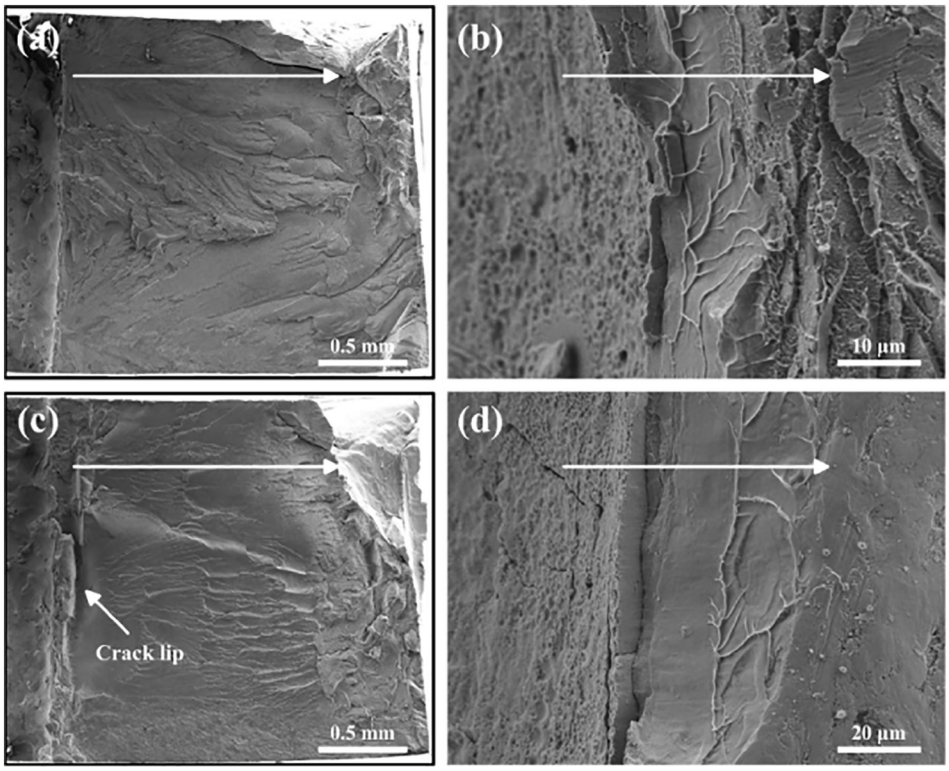

Fig. 5. SEM images of the fracture morphology of as-cast and pre-compressed specimens. The white arrows indicate the crack propagation direction. (a) and (c) Fracture surfaces of the as-cast and pre-compressed specimens, respectively. (b) and (d) Shear-sliding zones and viscous fingering without cavitation in plain-stress regions of the as-cast and pre-compressed specimens, respectively.

along the pre-existing shear band (as shown by green arrows) beyond the plastic zone can enhance the fracture resistance. However, as shown in Fig. 4(d), there secondary shear bands are neither branched nor extended, proved by the ends of secondary shear bands (marked by the blue circles) and branch point of shear bands (marked by the blue boxes). This indicates that the pre-existing main shear band can lead to the bifurcation of the crack. Therefore, the process of crack deflection from one pre-existing shear band to another one causes the significant crack blunting by shear sliding [37].

Shear band is a form of plastic instability that localizes large strains in a relatively thin band when a material is deformed. Considering the deformation behavior of metallic glasses, the key is to fully understand shear bands, their initiation, propagation, evolution, consequences, and control. The plastic deformation of metallic glasses on the macroscopic scale is essentially a biased accumulation of local strains incurred through the operation of shear transformation zones (STZs) and the redistribution of free volume [1,38–40]. Therefore, as the loading is increased on metallic glasses, more shear transformations will be activated. Once the stress reaches a critical value, the shear bands will initiate from a collection of STZs [38]. However, the molecular dynamics simulation indicates that the plastic deformation is driven by the random movement of atoms [41]. The present strategy is to introduce pre-existing shear bands near notch root to provide internal weak interfaces in ZC BMG that will guide and deflect evolving cracks, thereby increasing the crack resistance [26]. Deflection of cracking to regions that lie outside the plastic zone where stresses are lower should inhibit cavitation and further increase the toughness [36,42]. Therefore, if pre-existing shear bands can be locally introduced into BMGs that exceed the plastic zone size of the original material, crack deflection beyond the plastic zone will be promoted [26].

The crack-lip features are not obvious on the fracture surface of as-cast sample (Fig. 5(a)). However, the crack-lip size at the crack initiation locations in pre-compression sample is measured to be about 240 μm (Fig. 5(c)). The plane-strain plastic zone sizes R_p (= 123 μm) of the pre-compression sample is much smaller than that of the crack lip (Fig. 5(c)). This confirms that the crack in the plane-strain region also deflects beyond the plastic zone along pre-existing shear bands [26]. The smooth regions between the notch root and viscous fingering are measured to be 3 and 20 μm in width for as-cast and pre-compression sample (Fig. 5(b) and (d)), respectively. The smooth featureless shear-sliding zones, which correspond to about half of the notch opening displacement, are indicative of crack-tip blunting during crack propagation [43].

4. Conclusions

In summary, a pre-compression strategy is utilized for a ZC BMG to create pre-existing shear bands, guiding and deflecting cracks under dynamic condition. The pre-compressed specimen with a load of 2.5 kN had a dynamic notch toughness of 54.44 MPa·$m^{1/2}$, which is 18% higher than that of the as-cast ones. The pre-compression can effectively enhance the fracture toughness, since the pre-existing shear bands can guide and deflect cracks upon quasi-static and dynamic loadings. Furthermore, the crack can be deflected beyond the plastic zone size and propagate along the pre-existing main shear band. However, the crack of the as-cast specimen is not deflected beyond the plastic zone size. The smooth region of pre-compressed specimens is apparently larger than that of as-cast ones, indicating the crack-tip blunting during crack propagation.

Acknowledgments

This work is supported by the National Natural Science Foundation of China (Grant No. 11390362), the Top Young Academic Leaders of Shanxi and the Outstanding Innovative Teams of Higher Learning Institutions of Shanxi. The financial contributions are gratefully acknowledged.

References

[1] C.A. Schuh, T.C. Hufnagel, U. Ramamurty, Acta Mater. 55 (2007) 4067–4109.
[2] T. Egami, T. Iwashita, W. Dmowski, Metals 3 (2013) 77–113.
[3] B.A. Sun, W.H. Wang, Prog. Mater. Sci. 74 (2015) 211–307.

[4] S.V. Madge, Metals 5 (2015) 1279–1305.
[5] M.M. Trexler, N.N. Thadhani, Prog. Mater. Sci. 55 (2010) 759–839.
[6] J.J. Kruzic, Adv. Eng. Mater. 18 (2016) 1308–1331.
[7] R. Narasimhan, P. Tandaiya, I. Singh, R.L. Narayan, U. Ramamurty, Int. J. Fract. 191 (2015) 53–75.
[8] J. Xu, U. Ramamurty, E. Ma, JOM 62 (2010) 10–18.
[9] M.E. Launey, R.O. Ritchie, Adv. Mater. 21 (2009) 2103–2110.
[10] S.H. Xie, J.J. Kruzic, J. Alloys Compd. 694 (2017) 1109–1120.
[11] M.D. Demetriou, M.E. Launey, G. Garrett, J.P. Schramm, D.C. Hofmann, W.L. Johnson, R.O. Ritchie, Nat. Mater. 10 (2011) 123–128.
[12] D.C. Hofmann, J.Y. Suh, A. Wiest, M.L. Lind, M.D. Demetriou, W.L. Johnson, Proc. Natl. Acad. Sci. U. S. A. 105 (2008) 20136–20140.
[13] D.C. Hofmann, J.Y. Suh, A. Wiest, G. Duan, M.L. Lind, M.D. Demetriou, W.L. Johnson, Nature 451 (2008) 1085–1089.
[14] J.J. Lewandowski, M. Shazly, A.S. Nouri, Scr. Mater. 54 (2006) 337–341.
[15] P. Tandaiya, U. Ramamurty, G. Ravichandran, R. Narasimhan, Acta Mater. 56 (2008) 6077–6086.
[16] Z.D. Zhu, P. Jia, J. Xu, Scr. Mater. 64 (2011) 785–788.
[17] J.W. Qiao, H.L. Jia, P.K. Liaw, Mater. Sci. Eng. R 100 (2016) 1–69.
[18] Y.J. Huang, Y. Sun, J. Shen, Intermetallics 18 (2010) 2044–2050.
[19] H. Huang, J.L. Zhang, C.H. Shek, J.W. Yan, J. Alloys Compd. 674 (2016) 223–228.
[20] J.L. Zhang, H.B. Yu, J.X. Lu, H.Y. Bai, C.H. Shek, Appl. Phys. Lett. 95 (2009) 071906.
[21] X.D. Yuan, S.H. Wang, K.K. Song, X.L. Han, Y.S. Qin, D.F. Li, X.L. Li, B. Song, H. Xing, L. Wang, J. Iron Steel Res. Int. 24 (2017) 402–410.
[22] S.D. Feng, L. Qi, G. Li, W. Zhao, R.P. Liu, J. Non-Cryst. Solids 373–374 (2013) 1–4.
[23] J. Kobata, T. Kimura, Y. Takigawa, T. Uesugi, H. Kimura, K. Higashi, Mater. Trans. 50 (2009) 2355–2358.
[24] Q.P. Cao, J.W. Liu, K.J. Yang, F. Xu, Z.Q. Yao, A. Minkow, H.J. Fecht, J. Ivanisenko, L.Y. Chen, X.D. Wang, S.X. Qu, J.Z. Jiang, Acta Mater. 58 (2010) 1276–1292.
[25] L. He, M.B. Zhong, Z.H. Han, Q. Zhao, F. Jiang, J. Sun, Mater. Sci. Eng. A 496 (2008) 285–290.
[26] J. Yi, W.H. Wang, J.J. Lewandowski, Adv. Eng. Mater. 17 (2015) 620–625.
[27] G. Sunny, V. Prakash, J.J. Lewandowski, Metall. Mater. Trans. A 44 (2013) 4644–4653.
[28] K. Fujita, A. Okamoto, N. Nishiyama, Y. Yokoyama, H. Kimura, A. Inoue, J. Alloys Compd. 434–435 (2007) 22–27.
[29] D.L. Henann, L. Anand, Acta Mater. 57 (2009) 6057–6074.
[30] F.C. Jiang, R.T. Liu, X.X. Zhang, K.S. Vecchio, A. Rohatgi, Eng. Fract. Mech. 71 (2004) 279–287.
[31] L. Rubio, J. Fernandez-Saez, C. Navarro, Exp. Mech. 43 (2003) 379–386.
[32] J.W. Dally, D.B. Barker, Exp. Mech. 28 (1988) 298–303.
[33] W.G. Guo, Y.L. Li, Y.Y. Liu, Theor. Appl. Fract. Mech. 26 (1997) 29–34.
[34] X.K. Zhu, J.A. Joyce, Eng. Fract. Mech. 85 (2012) 1–46.
[35] Y. Zhang, W.H. Wang, A.L. Greer, Nat. Mater. 5 (2006) 857–860.
[36] H.J. Leamy, H.S. Chen, T.T. Wang, Metall. Mater. Trans. A 3 (1972) 699–708.
[37] P. Murali, T.F. Guo, Y.W. Zhang, R. Narasimhan, Y. Li, H.J. Gao, Phys. Rev. Lett. 107 (2011) 215501.
[38] A.L. Greer, Y.Q. Cheng, E. Ma, Mater. Sci. Eng. R 74 (2013) 71–132.
[39] C.A. Schuh, A.C. Lund, Nat. Mater. 2 (2003) 449–452.
[40] Q.K. Li, M. Li, Appl. Phys. Lett. 88 (2006) 241903.
[41] N. Yedla, S. Ghosh, Intermetallics 80 (2017) 40–47.
[42] Q. He, J.K. Shang, E. Ma, J. Xu, Acta Mater. 60 (2012) 4940–4949.
[43] A. Tatschl, C.J. Gilbert, V. Schroeder, R. Pippan, R.O. Ritchie, J. Mater. Res. 15 (2000) 898–903.